Benchmarking of three-dimensional multicomponent lattice Boltzmann equation

XU, Xu <http://orcid.org/0000-0002-9721-9054>, BURGIN, Kallum, ELLIS, M and HALLIDAY, Ian <http://orcid.org/0000-0003-1840-6132>

Benchmarking of Three-Dimensional Multi-Component Lattice Boltzmann Equation

X. Xu [1,2], K. Burgin [1], M. A. Ellis [3], and I. Halliday [1]
[1] *Materials & Engineering Research Institute, Sheffield Hallam University, Howard Street, S1 1WB (UK)*
[2] *Department of Engineering and Mathematics, Sheffield Hallam University, Howard Street, S1 1WB (UK) and*
[3] *Oriel College, University of Oxford, OX1 4EW (UK)*
(Dated: October 26, 2017)

We present a challenging validation of phase field multi-component lattice Boltzmann equation (MCLBE) simulation against the Re = 0 Stokes flow regime Taylor-Einstein theory of dilute suspension viscosity. By applying a number of recent advances in the understanding and the elimination of the interfacial micro-current artefact, extending to 3D a class of stability-enhancing multiple relaxation time collision models (which require no explicit collision matrix, note) and developing new interfacial interpolation schemes, we are able to obtain data which show that MCLBE may be applied in new flow regimes. Our data represent one of the most stringent tests yet attempted on LBE—one which received wisdom would preclude on grounds of overwhelming artefact flow.

I. INTRODUCTION

The past two decades have seen steady growth in interest in multi-relaxation time (MRT) lattice Boltzmann (LB) schemes which offer enhanced simulation stability [1], [2], [3], [4], [5], [6], [7] and [8] etc. We extend to D3Q19 a recent D2Q9 variant [9], in which the usual collision matrix is only implicit, being represented by a carefully chosen, modal eigen-basis which is subject to forced, scalar relaxation. As well as the usual advantages, the new method has transparent analytic properties: its orthogonal modes are defined as polynomials in the lattice basis, as are the elements of the transformation matrix between the distribution function and the mode space. This uniquely allows for the direct reconstruction of a post-collision distribution function, which is effectively parameterized by the eigenvalue spectrum. Our purpose in developing a new model is to stabilize multi-component LBE (MCLBE) so as to attempt the challenge of recovering the Taylor-Einstein theory of suspension viscosity [10], [11].

The structure of this paper is as follows. In section II, we provide background material of the proposed 3D MRT scheme. In section III, we present relevant methodological advances, in particular, the discovery of 19 polynomial expressions for the inverse transformation matrix, and the analysis of different viscosity interpolation methods. In section IV, we illustrate and discuss the theoretical and simulation results achieved and finally, in section V, we conclude on the significant findings of this work.

II. BACKGROUND

First, consider the base model. Our 3D MRT LBE with body force, $\mathbf{F}$, may be written:

$$f_i\left(\mathbf{x}+\mathbf{c_i}\delta t, t+\delta t\right) = f_i(\mathbf{x},t) + \sum_j A_{ij}\left[f_j^{(0)}(\mathbf{x},t) - f_j(\mathbf{x},t)\right] + \delta t F_i, \quad (1)$$

where

$$F_i = t_i\left[3\mathbf{F}\cdot\mathbf{c}_i + \frac{9}{2}\left(1-\frac{\lambda_3}{2}\right)\left(F_\alpha u_\beta + F_\beta u_\alpha\right)\right], \quad (2)$$

and

$$f_j^{(0)} = \rho t_j\left(1 + 3u_\alpha c_{j\alpha} + \frac{9}{2}u_\alpha u_\beta c_{j\alpha}c_{j\beta} - \frac{3}{2}u_\gamma u_\gamma\right). \quad (3)$$

To recover hydrodynamics, F_i, collision matrix $\mathbf{A}$, and its eigenvalues λ_i, must preserve the following properties:

$$\begin{aligned}
&\sum_i F_i = 0, \sum_i \mathbf{c}_i F_i = n\mathbf{F}, \sum_i \mathbf{c}_i\mathbf{c}_i F_i = \frac{1}{2}\left[\mathbf{C}+\mathbf{C^T}\right],\\
&\sum_i 1_i A_{ij} = 0, \sum_i c_{i\alpha}A_{ij} = 0, \sum_i g_i A_{ij} = \lambda_{10} g_j,\\
&\sum_i c_{i\alpha}c_{i\beta}A_{ij} = \lambda_4 c_{j\alpha}c_{j\beta}, \sum_i g_i c_{i\alpha}A_{ij} = \lambda_{11} g_j c_{j\alpha},\\
&\sum_i c_{i\alpha}^2 c_{i\beta}A_{ij} = \lambda_{14} c_{j\alpha}^2 c_{j\beta}, \sum_i g_i c_{i\alpha}^2 A_{ij} = \lambda_{17} g_j c_{j\alpha}^2, \quad (4)
\end{aligned}$$

where α and β represent the x, y or z directions, λ_p denotes the pth eigenvalue of A_{ij}, and $C_{\alpha\beta} \equiv \frac{1}{2}\left(u_\alpha F_\beta + u_\beta F_\alpha\right)$ [9]. For eigenvalues, their corresponding left-row eigenvectors, $\mathbf{h}^{(p)}$, $p \in [0, 18]$, and the modes they project, see Table I (a). $\mathbf{A}$ is defined by its eigenspectrum $(\mathbf{h}^{(p)}, \lambda^{(p)})$ which project modes with scalar relaxation.

III. METHODOLOGY

A. Explicit Algebraic 3D MRT Scheme

For D3Q19, we extend the set developed for D2Q9 [9], using Gram-Schmidt orthogonalisation to which in Table I (a). Four degenerate eigenvectors necessarily project hydrodynamic modes $\rho \equiv \sum_i f_i$ and $\rho\mathbf{u} \equiv \sum_i f_i\mathbf{c}_i$ [9] with $\lambda_i = 0$, six project components of stress $P_{\alpha\beta}$, four "ghosts" are chosen to project N, $\mathbf{J}$ (following

Benzi et. al [2], [3] and Dellar [4]) and five new eigenvectors are denoted E_1, E_2, E_3, X_x and X_y. Left-row eigenvectors $\mathbf{h}^{(p)}s$ define projection matrix:

$$\mathbf{M} \equiv \Big(\mathbf{h}^{(0)}, \mathbf{h}^{(1)}, \cdots, \mathbf{h}^{(18)}\Big)^T \tag{5}$$

such that:

$$\mathbf{M}\ \mathbf{f} = \big(\rho, \rho u_x, \rho u_y, \rho u_z, P_{xx}, P_{yy}, P_{zz}, P_{xy}, P_{xz}, P_{yz}, N, J_x, J_y, J_z, E_1, E_2, E_3, X_x, X_y\big)^T, \tag{6}$$

where $\mathbf{f} \equiv (f_0, f_1, f_2, \ldots, f_{18})^T$. Using $\mathbf{M}$, Eq. (1) may be transformed:

$$\mathbf{M}\ \mathbf{f}^+ = \mathbf{M}\ \mathbf{f} + \mathbf{M}\ \mathbf{A}\ \mathbf{M^{-1}}\Big(\mathbf{M}\ \mathbf{f^{(0)}} - \mathbf{M}\ \mathbf{f}\Big) + \mathbf{M}\tilde{\mathbf{F}}, \tag{7}$$

where $\tilde{\mathbf{F}}$ denotes a column vector with elements F_i and $\mathbf{f}$, $\mathbf{f}^+$ and $\mathbf{f}^{(0)}$ are now column vectors. Since the $\mathbf{h}^{(p)}$ are left row eigenvectors of $\mathbf{A}$, it follows:

$$\mathbf{M}\ \mathbf{A} = \mathbf{\Lambda}\ \mathbf{M} \ \Leftrightarrow\ \mathbf{\Lambda} = \mathbf{M}\ \mathbf{A}\ \mathbf{M^{-1}}, \tag{8}$$

where $\mathbf{\Lambda} = diag(\lambda_0,\ \lambda_1,\ \cdots\ \lambda_{18})$. Therefore Eq. (1) may be written in mode space as:

$$\mathbf{h}^{(p)+} = \mathbf{h}^{(p)} + \lambda_p\Big(\mathbf{s}^{(p)} - \mathbf{h}^{(p)}\Big) + \mathbf{S}^{(p)}, \tag{9}$$

where $\mathbf{S}^{(p)} \equiv \mathbf{M}\cdot\tilde{\mathbf{F}}$ and $\mathbf{s}^{(p)} \equiv \mathbf{M}\cdot\mathbf{f}^{(0)}$. The inverse transformation matrix:

$$\mathbf{M}^{-1} \equiv \Big(\mathbf{k}^{(0)}, \mathbf{k}^{(1)}, \mathbf{k}^{(2)}, ..., \mathbf{k}^{(18)}\Big) \tag{10}$$

may be constructed from column vectors $\mathbf{k}^{(p)}$, exactly defined as polynomials of the lattice basis, such that:

$$6k_i^{(0)} = t_i\big[12g_ic_{i\theta}^2 - 15c_{i\theta}^2 - 21c_{iz}^2 + 23 - 8g_i\big], \tag{11}$$

$$k_i^{(1)} = t_i\big[6c_{ix}c_{iy}\left(2c_{ix} - c_{iy}\right) + c_{ix}(5 + g_i) - 2c_{iy}(2 - g_i)\big], \tag{12}$$

$$k_i^{(2,3)} = t_ic_{i\gamma}\big[5 + g_i - 6c_{ix}^2\big], \tag{13}$$

$$2k_i^{(4,5)} = t_i\big[-2g_i\left(c_{i\zeta}^2 + 2c_{i\xi}^2\right) + 11c_{i\zeta}^2 + c_{i\xi}^2 + 3c_{iz}^2 - 5 + 2g_i\big], \tag{14}$$

$$2k_i^{(6)} = t_i\big[-6g_ic_{i\theta}^2 + 3c_{i\theta}^2 + 15c_{iz}^2 - 7 + 4g_i\big],$$

$$k_i^{(7,\cdots,9)} = 3t_ic_{i\alpha}c_{i\beta}, \tag{15}$$

$$2k_i^{(10)} = t_i\big[6c_{i\theta}^2 - 12g_ic_{i\theta}^2 + 12c_{iz}^2 - 8 + 11g_i\big], \tag{16}$$

$$k_i^{(11)} = t_i\big[3c_{ix}c_{iy}\left(2c_{ix} - c_{iy}\right) + c_{ix}(1 + 2g_i) - c_{iy}(2 + g_i)\big], \tag{17}$$

$$k_i^{(12,13)} = 2t_ig_ic_{i\gamma}\big[2 + 4g_i - 6c_{ix}^2\big], \tag{18}$$

$$k_i^{(14,15)} = 3t_ic_{i\gamma}\big[6c_{ix}^2 - 2 - g_i\big], \tag{19}$$

$$k_i^{(16)} = 3t_i\big[6c_{ix}c_{iy}\left(c_{iy} - 2c_{ix}\right) - (2 + g_i)(c_{ix} - 2c_{iy})\big], \tag{20}$$

$$k_i^{(17)} = t_i\big[-g_i\left(4c_{ix}^2 + c_{iy}^2\right) - c_{ix}^2 - 2c_{iy}^2 - 3c_{iz}^2 + 2 - 2g_i\big], \tag{21}$$

$$k_i^{(18)} = t_i\big[2g_i\left(c_{ix}^2 + 2c_{iy}^2\right) - 2c_{ix}^2 - c_{iy}^2 - 3c_{iz}^2 + 2 - 2g_i\big], \tag{22}$$

where $c_{i\theta}^2 = c_{ix}^2 + c_{iy}^2$, $\gamma \in [y, z]$ and is taken in alphabetical order, (ζ, ξ) are taken in order as (x, y) and (y, x), and $\alpha, \beta \in [x, y, z]$ and are denoted in the pair order of (x, y), (x, z) and (y, z). Using the methodology developed for the D2Q9 case [9], we invert $\mathbf{M}$ to construct a post-collision distribution function vector $\mathbf{f}^+$, describing flow in the presence of force distribution, $\mathbf{F}$:

$$\mathbf{f}^+ = \mathbf{M}^{-1}\big(\rho^+, \rho u_x^+, \rho u_y^+, \rho u_z^+, P_{xx}^+, P_{yy}^+, P_{zz}^+, P_{xy}^+, P_{xz}^+, P_{yz}^+, N^+, J_x^+, J_y^+, J_z^+, E_1^+, E_2^+, E_3^+, X_x^+, X_y^+\big)^T, \tag{23}$$

which may be written in explicit form after [9]. MRT LBE is more computationally expensive than LBGK [12] but is more stable [1], [2], [3]. The novelty of the scheme we extend here from [9] includes the existence of polynomial expressions $\mathbf{k}^{(p)}$ which allow (i) algebraic inversion from the mode space (Eq. (10)), (ii) an exact expression for $\mathbf{f}^+$, (iii) removal of explicit collision and inversion matrices, and hence some computational overhead.

B. Interfacial Viscosity Interpolation

Here we are motivated by a need to extend the viscosity contrast available in simulations of multi-component flow using a phase-field MCLBE [9], [13], [14], to facilitate a validation against the stress field Taylor predicted in 1932, for steady, shear flow past a spherical drop at Re = 0 [10] and the consequent prediction of effective viscosity in a dilute suspension of small drops, after Einstein [11]. Accordingly,

$$\mathbf{F} = \frac{\sigma\kappa}{2}\nabla\rho^N \tag{24}$$

is an immersed boundary force, where according to [15], the phase field is:

$$\rho^N \equiv \frac{\rho_R - \rho_B}{\rho_R + \rho_B}, \tag{25}$$

and the local interfacial curvature is:

$$\kappa \equiv \nabla_s\frac{\nabla\rho^N}{|\nabla\rho^N|}. \tag{26}$$

Here, ρ_R, ρ_B are densities of two immiscible fluid components, which are segregated, post collision, using the methodology of d'Ortona [16] (see [9], [13], [14]) and ∇_s is a surface gradient operator.

The above force field is localised but clearly continuously distributed. In fact, in all MCLBE an interface is defined by a phase field or order parameter which varies continuously, over a small distance, between constant bulk fluids values, with a continuum interface commonly taken to be $\rho_N = 0$ surface. The finite width of the resulting interface calls into question the representation

of target continuum-scale kinematic and dynamic conditions. In the present context, we are concerned with the no-traction condition [22].

Take a steady, planar, red-blue interface $x = x_0$, constant, sheared in y direction, after Liu et al. [23]. Phase field MCLBE is described by a weakly compressible Navier-Stokes equation with $\mathbf{F}$, for what is a single, effective fluid (the role of $\mathbf{F}$ is to insert Laplace law physics). For a flat interface, $\mathbf{F} = \mathbf{0}$ and the lattice fluid is described by $\frac{d}{dx}\sigma'_{xy} = 0$, $\forall x$. Applying system symmetries, we obtain $\sigma'_{xy} = K$, a constant $\forall x$. This prefigures the continuum no-traction (continuity of viscous flux) condition. Apparently LBE's dynamics automatically ensure shear stress is continuous through the interface region. Clearly choice exists in the interpolation of viscosity or, equivalently λ_4. Liu and co-workers impose a requirement on the velocity gradient, that it varies like ρ^N [23], in this situation and in applications to contact angle hysteresis [24]. This assumption yields an interpolation of λ_4 derived from the a harmonic mean of viscosity with weights $\frac{\rho_R}{\rho}$ and $\frac{\rho_B}{\rho}$. Liu et al. [23] state their approach is equivalent to Ginzburg's, when projecting the sharp interface limit [25] (see Fig. 3 of [25]). Zu et al. [26] assume the interfacial velocity gradient follows an order parameter and argue for an interpolation based on a weighted arithmetic average of reciprocal viscosity. There are more involved approaches, including that of Grunau et al. [27]. For the data presented in the next section, optimum agreement with Taylor-Einstein theory is obtained using a novel method.

In our MCLBE, interfacial effects are carried by a force with weight $|\nabla\rho^N|$ which may be approximated by $\frac{4\rho_R\rho_B}{\rho^2} = (1 - \rho^{N2})$ [28]. Self-consistency argues for an interpolation of λ_4, between bulk values λ_4^R and λ_4^B, such that source term, F_i, has a consistent variation. Hence, we choose $\left(1 - \frac{\lambda_4}{2}\right) \sim \rho^N$ or $\left(1 - \frac{\bar{\lambda}_4}{2}\right) = \frac{\rho_R}{\rho}\left(1 - \frac{\lambda_4^R}{2}\right) + \frac{\rho_B}{\rho}\left(1 - \frac{\lambda_4^B}{2}\right)$, and noting $\frac{\rho_R}{\rho} + \frac{\rho_B}{\rho} = 1$, our interpolation may be written:

$$\bar{\lambda}_4 = \frac{\rho_R}{\rho}\lambda_4^R + \frac{\rho_B}{\rho}\lambda_4^B = \frac{1+\rho^N}{2}\lambda_4^R + \frac{1-\rho^N}{2}\lambda_4^B. \quad (27)$$

In section IV we will consider data derived from the above interpolation alongside that obtained using other methods. The different interpolations used for reference in section IV are based on taking a relative density weighted harmonic mean of shear viscosity $\eta = \frac{\rho}{\frac{\rho_R}{\eta_R} + \frac{\rho_B}{\eta_B}}$ which may be expressed as follows:

$$\frac{\bar{\lambda}_4}{2 - \bar{\lambda}_4} = \frac{\rho_R}{\rho}\left(\frac{\lambda_4^R}{2 - \lambda_4^R}\right) + \frac{\rho_B}{\rho}\left(\frac{\lambda_4^B}{2 - \lambda_4^B}\right), \quad (28)$$

and also an interpolation based on the arithmetic mean of shear viscosity $\eta = \frac{\rho_R}{\rho}\eta_R + \frac{\rho_B}{\rho}\eta_B$, which may be expressed as:

$$\frac{1}{\bar{\lambda}_4} = \frac{\rho_R}{\rho}\frac{1}{\lambda_4^R} + \frac{\rho_B}{\rho}\frac{1}{\lambda_4^B}. \quad (29)$$

IV. RESULTS AND DISCUSSION

Experimental studies of suspension viscosity emphasise concentration values outside the Re = 0 theory but do identify certain emulsions which behave in agreement with the Taylor-Einstein result, certainly for concentrations $c < 5\%$ (see e.g. Nawab et al. [17], Hur et al. [18] and Mason et al. [19]). Notably, a comparison of MCLBE with Re = 0 theory is not obstructed by MCLBE's notorious interfacial micro-current (see [20] and references therein). For phase-field MCLBE variants, this artefact has recently been argued to arise from superposable solutions to the field equations, attributable, in increasing significance, to the stencil used for force weight $\nabla\rho^N$, discrete lattice effects and (most significantly) the calculation of κ [20]. At Re = 0, hydrodynamic signals cannot be assumed to overwhelm artefacts, but this regime may still be addressed by subtracting independent micro-current fields, to expose a hydrodynamic response. (Micro-current fields are easily determined for a red drop in stationary blue fluid.)

Fig. 1 compares stresses between theory and micro-current adjusted simulation. We show viscous stress σ'_{xy} measured in the projected equatorial plane, $z = 0$, of a three-dimensional red drop, initial radius $R = 20$ lattice units, contained within a cubic box, side L lattice units, with the continuous component (blue) fluid subject to a Lees-Edwards shear [21]. This boundary condition eliminates finite size effects but allows periodic drop replicas to interact [9]. The resulting suspension concentration is controlled by L, i.e.

$$c = \frac{4\pi R^3}{3L^3}. \quad (30)$$

The applied shear corresponds to approximately constant boundary flow parallel to $\hat{e}_y$ in box faces $x = x_0$, constant. Taylor calculated $\sigma'^{(T)}_{\alpha\beta}$, $\alpha, \beta \in [x, y, z]$ due to an inclined, applied shear, superposed with a constant body rotation around $\hat{e}_z$ [10]. Accordingly, to compare with our simulation, it is necessary to rotate co-ordinates and in Fig. 1 panel (a) shows a combination of Taylor's stresses $\left(\sigma'^{(T)}_{xx} - \sigma'^{(T)}_{yy}\right)$. Figs. 1(b)..(d) show the corresponding simulation data for $L = 128$, viscosity contrast:

$$\Lambda \equiv \frac{\eta_R}{\eta_B}, \quad (31)$$

where η_C is the shear viscosity of the C fluid. In Fig. 1 we show the significant difference between stress fields measured using existing and novel interfacial interpolations of viscosity, or equivalently, λ_4. These are given in Eqs. (27), (28) and (29). Furthermore, the viscous stress field, σ'_{xy}, is shown in Fig. 1 for two Λ. For this data $\eta_B = \frac{1}{3}$ (the continuous component) is fixed and $\frac{R}{L} = \frac{1}{6}$. For the images in the upper row, $\Lambda = \frac{1}{16}$. Panel (a) shows Taylor-Einstein theory, panel (b) shows the stress field obtained using the interfacial interpolation

based upon a density-weighted harmonic mean of separated fluids' parameter $\tau = \frac{1}{\lambda_4}$ (see Eq. (27)), panel (c) shows stress obtained with the interfacial interpolation based upon a density-weighted harmonic mean of shear viscosity (see Eq. (28)) and panel (d) shows results from our novel method of interfacial interpolation shear viscosity, based upon a density-weighted arithmetic mean of shear viscosity (see Eq. (29)). In the top row, it is clear that (b) are (d) are most representative of (a). The bottom row in Fig. 1 shows equivalent data for $\Lambda = 12$ and it clearly shows that (f) and (g) are most representative of (e).

We next consider a range of crystalline suspension concentrations, each of fixed viscosity ratio, Λ, inferring effective suspension viscosity, η_{eff}, from plots of system-averaged $\langle\sigma_{xy}\rangle$ against c, fitted using unconstrained regression (see e.g. Fig. 2). For micro-current flow alone, $\langle\sigma_{xy}\rangle \approx 0$ (though viscous dissipation is affected—see [9]) but it is still necessary to correct system $\langle\sigma_{xy}\rangle$ for the presence of immersed boundary force, $\mathbf{F}$ [9]. Agreement with Taylor-Einstein theory is affected by the method used to interpolate λ_4, or alternatively viscosity, η, in the inter-facial region, as we now discuss. All data in Figs. 2, 3 and 4 correspond to

$$\text{Re} \equiv \frac{\dot{\gamma}R^2\rho}{\eta} = 0.0198, \tag{32}$$

$$\text{Ca} \equiv \frac{\eta\dot{\gamma}R}{\sigma} = 0.0110, \tag{33}$$

which are held constant throughout.

Fig. 2 shows eleven sets of measured η_{eff} for a wide range of Λ such that $\frac{1}{32} \leq \Lambda \leq 12$ (crosses interpolated by dotted lines), and the appropriate Taylor-Einstein predictions (solid lines of same colour):

$$\eta_{\text{eff}}^{(T)} = \eta_B \left[1 + \left(\frac{\frac{5}{2}\Lambda + 1}{\Lambda + 1}\right) c\right]. \tag{34}$$

Data presented in Fig. 3 are equivalent to that shown in Fig. 2, but using different interfacial interpolation methods. Panel (a) in Fig. 3 shows effective suspension viscosity data based upon the interpolation of interfacial viscosity in Eq. (28), panel (b) shows equivalent data based upon Eq. (29). The quality of the fit to theory with the different interpolation methods is different over different part over the domain of Λ. This is clearly shown in Fig. 4 where we show the relative error:

$$\epsilon \equiv \left(\frac{\eta_{\text{eff}}^{(T)} - \eta_{\text{eff}}}{\eta_{\text{eff}}^{(T)}}\right) \times 100\%, \tag{35}$$

plotted over the range of Λ. It is apparent that for $\Lambda > 1$, the agreement with theory using arithmetic mean method is significantly worse, whereas for $\Lambda < 1$, the agreement using harmonic mean method is much worse. Our interpolation in Eq. (27) represents an optimum over the whole range of Λ. This point is further summarized in the section V.

V. CONCLUSIONS

Taken together, Figs. 1, 2, 3 and 4 underscore the significance of the interfacial interpolation. The fit produced by Eq. (27) represents an optimum over the range of Λ studied and is best when the exterior fluid is more viscous. For $\Lambda < 1$, the fit is improved by using an interpolation based upon an arithmetic mean of viscosities however the fit at $\Lambda > 1$ then degrades. Over the range of Λ, the scheme in Eq. (27) produced most consistent agreement.

Comparison with the Taylor-Einstein represents a stringent test of phase field MCLBE (and thereby the approximations within the theory [10] which, here, has been extended to fluid subject to an immersed boundary force [9]). It is facilitated by our development of an inverse MRT methodology—a generic scheme which circumvents the need for a calculation of collision matrix and allows direct construction of a post-collision LBE distribution function.

The conditions of our validation (Re, Ca small) mean the micro-current is significant with respect of physical flow (possibly the reason for previous neglect of this validation). Our results achieve a paradoxical accuracy resolved by appealing to recent work on the hydrodynamic nature of micro-current flow [20], the accuracy of the Taylor-Einstein result recovered herein may be understood by observing that $\text{Re} = 0$ regime is linear and micro-current stresses (themselves a solution of the Stokes equation) therefore superpose with flow induced by the applied shear. Once identified, they may be subtracted. Furthermore, this work points to the importance of the method of interpolation of viscosity eigenvalue, λ_4, across the interfacial region, with our data producing a optimum for the interpolation in Eq. (27).

Acknowledgments One of us (M.A.E) gratefully acknowledges financial support from the Engineering and Physical Sciences Research Council, Swindon, UK via Collaborative Computational Project 5 and Oriel College, University of Oxford.

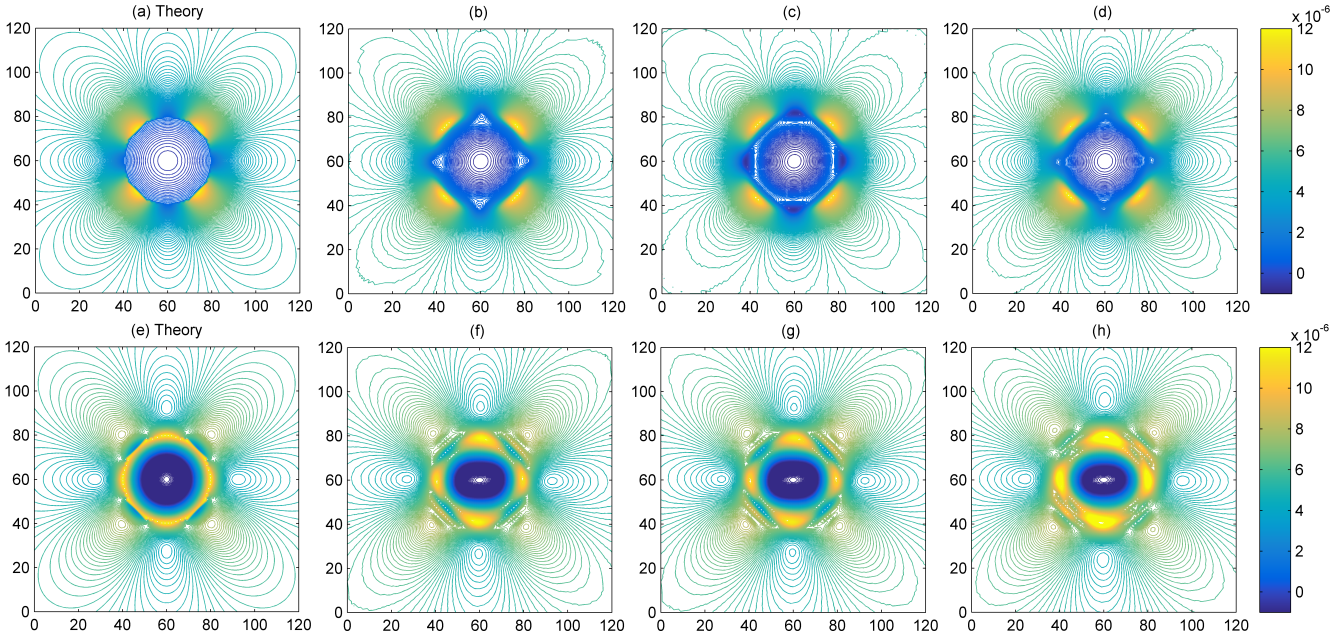

FIG. 1. Viscous stress field σ'_{xy} in the equatorial plane of a spherical red drop, radius $R = 20$, suspended in a blue fluid which is sheared, at $\mathrm{Re} = 0$ for two viscosity ratios, Λ, with $\eta_B = \frac{1}{3}$ (continuous component) and $\frac{R}{L} = \frac{1}{6}$. **Case 1,** $\Lambda = \frac{1}{16}$: (a) Taylor's theory, (b) inter-facial interpolation based upon a density-weighted harmonic mean of separated fluids' parameter $\tau = \frac{1}{\lambda_4}$ (see Eq. (27)), (c) inter-facial interpolation based upon a density-weighted harmonic mean of shear viscosity (see Eq. (28)), and (d) inter-facial interpolation based upon a density-weighted arithmetic mean of shear viscosity (see Eq. (29)). **Case 2,** $\Lambda = 12$: (e) Taylor's theory, (f) inter-facial interpolation based upon a density-weighted harmonic mean of separated fluids' parameter $\tau = \frac{1}{\lambda_4}$ (see Eq. (27)), (g) inter-facial interpolation based upon a density-weighted harmonic mean of shear viscosity (see Eq. (28)), and (h) inter-facial interpolation based upon a density-weighted arithmetic mean of shear viscosity (see Eq. (29)).

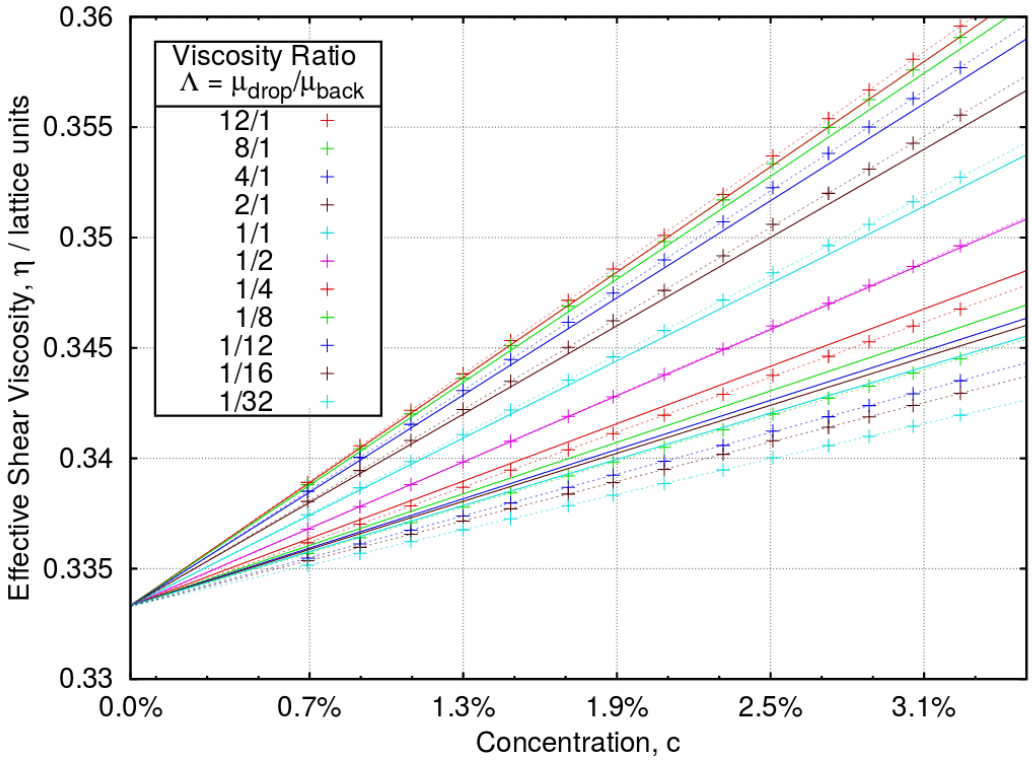

FIG. 2. Effective suspension viscosity, η_{eff}, as a function of concentration, c (discrete crosses linearly interpolated by dotted lines) for the indicated range of drop / background fluid viscosity ratio, $\Lambda = \frac{\eta_R}{\eta_B}$, together with the variation predicted by the Taylor-Einstein result, $\eta_{\text{eff}}^{(T)} = \eta_B \left[1 + \left(\frac{\frac{5}{2}\eta_R + \eta_B}{\eta_R + \eta_B}\right) c\right]$ (continuous line of corresponding colour). These data were obtained using the interpolation defined in Eq. (27).

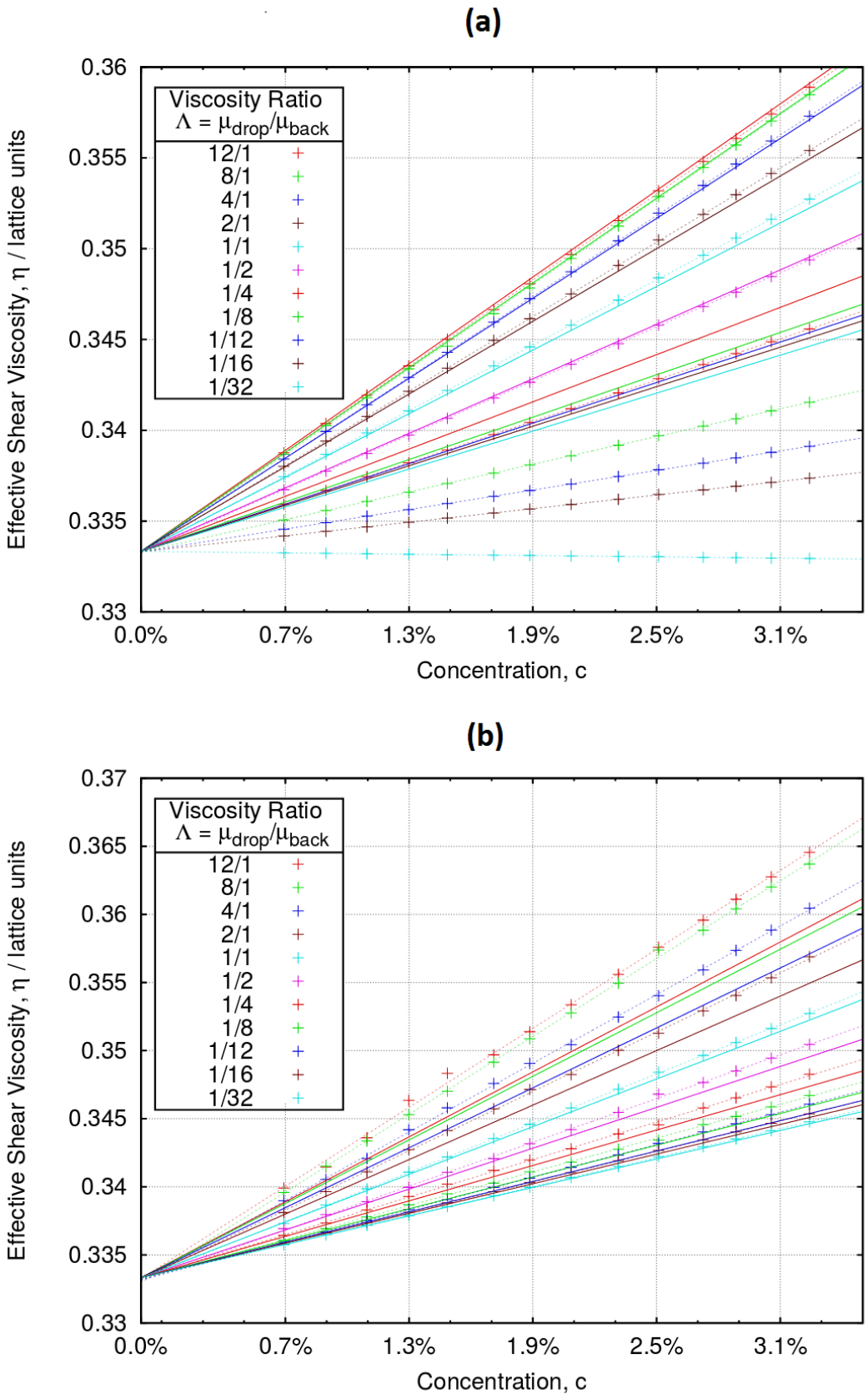

FIG. 3. Data equivalent to that shown in Fig. 2 using different interfacial interpolation methods. Effective suspension viscosity, η_{eff}, as a function of concentration, c (discrete crosses linearly interpolated by dotted lines) for the indicated range of drop / background fluid viscosity ratio, $\Lambda = \frac{\eta_R}{\eta_B}$, together with the variation predicted by the Taylor-Einstein result, $\eta_{\text{eff}}^{(T)} = \eta_B \left[1 + \left(\frac{\frac{5}{2}\eta_R + \eta_B}{\eta_R + \eta_B}\right) c\right]$ (continuous line of corresponding colour). These data were obtained using an interpolation based upon (a) the harmonic mean of the separated fluids' shear viscosity defined in Eq. (28) and (b) the arithmetic mean of shear viscosity defined in Eq. (29).

(a)						(b)			
mode	component	λ_p	projection	modal source, $S^{(p)}$	equilibrium, $s^{(p)}$	direction, i	c_{ix}	c_{iy}	c_{iz}
$\mathbf{h}^{(0)}$	$h_i^{(0)} = 1_i$	0	ρ	0	ρ	0	0	0	0
$\mathbf{h}^{(1)}$	$h_i^{(1)} = c_{ix}$	0	ρu_x	$nF_x\delta_t$	ρu_x	1	1	0	0
$\mathbf{h}^{(2)}$	$h_i^{(2)} = c_{iy}$	0	ρu_y	$nF_y\delta_t$	ρu_y	2	1	-1	0
$\mathbf{h}^{(3)}$	$h_i^{(3)} = c_{iz}$	0	ρu_z	$nF_z\delta_t$	ρu_z	3	0	-1	0
$\mathbf{h}^{(4)}$	$h_i^{(4)} = c_{ix}^2$	λ_4	P_{xx}	$\frac{1}{2}(C_{xx} + C_{xx})$	$\Pi_{xx}^{(0)}$	4	-1	-1	0
$\mathbf{h}^{(5)}$	$h_i^{(5)} = c_{iy}^2$	λ_4	P_{yy}	$\frac{1}{2}(C_{yy} + C_{yy})$	$\Pi_{yy}^{(0)}$	5	-1	0	0
$\mathbf{h}^{(6)}$	$h_i^{(6)} = c_{iz}^2$	λ_4	P_{zz}	$\frac{1}{2}(C_{zz} + C_{zz})$	$\Pi_{zz}^{(0)}$	6	-1	1	0
$\mathbf{h}^{(7)}$	$h_i^{(7)} = c_{ix}c_{iy}$	λ_4	P_{xy}	$\frac{1}{2}(C_{xy} + C_{yx})$	$\Pi_{xy}^{(0)}$	7	0	1	0
$\mathbf{h}^{(8)}$	$h_i^{(8)} = c_{ix}c_{iz}$	λ_4	P_{xz}	$\frac{1}{2}(C_{xz} + C_{zx})$	$\Pi_{xz}^{(0)}$	8	1	1	0
$\mathbf{h}^{(9)}$	$h_i^{(9)} = c_{iy}c_{iz}$	λ_4	P_{yz}	$\frac{1}{2}(C_{yz} + C_{zy})$	$\Pi_{yz}^{(0)}$	9	0	0	1
$\mathbf{h}^{(10)}$	$h_i^{(10)} = g_i$	λ_{10}	N	0	0	10	1	0	1
$\mathbf{h}^{(11)}$	$h_i^{(11)} = g_i c_{ix}$	λ_{11}	J_x	0	0	11	0	1	1
$\mathbf{h}^{(12)}$	$h_i^{(12)} = g_i c_{iy}$	λ_{11}	J_y	0	0	12	-1	0	1
$\mathbf{h}^{(13)}$	$h_i^{(13)} = g_i c_{iz}$	λ_{11}	J_z	0	0	13	-1	0	1
$\mathbf{h}^{(14)}$	$h_i^{(14)} = c_{ix}^2 c_{iy}$	λ_{14}	E_1	$\frac{1}{3}F_y$	$E_1^{(0)} = \frac{1}{3}\rho u_y$	14	0	0	-1
$\mathbf{h}^{(15)}$	$h_i^{(15)} = c_{ix}^2 c_{iz}$	λ_{14}	E_2	$\frac{1}{3}F_z$	$E_2^{(0)} = \frac{1}{3}\rho u_z$	15	1	0	-1
$\mathbf{h}^{(16)}$	$h_i^{(16)} = c_{ix}c_{iy}^2$	λ_{14}	E_3	$\frac{1}{3}F_x$	$E_3^{(0)} = \frac{1}{3}\rho u_x$	16	0	1	-1
$\mathbf{h}^{(17)}$	$h_i^{(17)} = g_i c_{ix}^2$	λ_{17}	X_x	$\left(1 - \frac{\lambda_4}{2}\right)(F_y u_y + F_z u_z)$	$X_x^{(0)} = \frac{\rho}{2}(u_y^2 + u_z^2)$	17	-1	0	-1
$\mathbf{h}^{(18)}$	$h_i^{(18)} = g_i c_{iy}^2$	λ_{17}	X_y	$\left(1 - \frac{\lambda_4}{2}\right)(F_x u_x + F_z u_z)$	$X_y^{(0)} = \frac{\rho}{2}(u_x^2 + u_z^2)$	18	0	-1	-1

TABLE I. (a) Collision matrix left-row eigenvector notation and properties, with eigenvalues and the corresponding equilibria and sources used in Eq. (9). Here, ρu_α, $P_{\alpha\beta}$, and $\Pi_{\alpha\beta}^{(0)}$ represent the α and $\alpha\beta$ components of momentum, viscous stress tensor, and momentum flux tensor, respectively. (b) The lattice basis or unit cell set for the D3Q19 model developed in this paper.

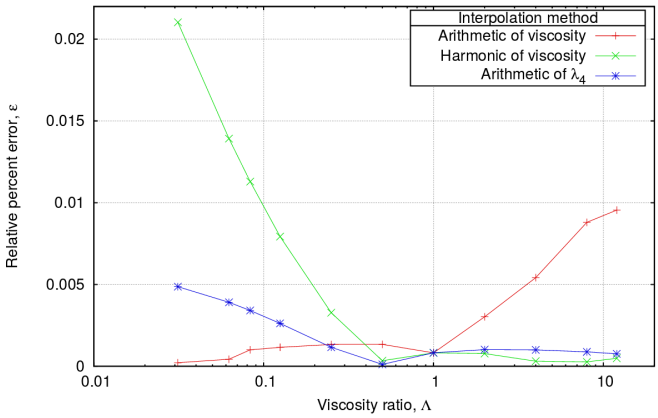

FIG. 4. Relative error of interfacial interpolation method, ϵ, for a range of Λ, expressed in %. For all data in Fig. 2, $\epsilon \equiv \frac{\eta_{\rm eff}^{(T)} - \eta_{\rm eff}}{\eta_{\rm eff}^{(T)}} \times 100\%$ was computed for each of the three interfacial interpolation methods considered, as identified in the key.

[1] P. Lallemand and L.-S. Luo, Phys. Rev. E 61, 6546, (2000).
[2] R. Benzi, S. Succi and M. Vergassola, Europhys. Lett. 13, pp727 (1990).
[3] R. Benzi, S. Succi and M. Vergassola, Phys. Rep. 222, pp145 (1992).
[4] P. J. Dellar Phys. Rev. E. 65, 036309 (2002).
[5] M. E. McCracken and J. Abraham, Phys. Rev. E 71(3), 036701 (2005).
[6] K. N. Premnath and J. Abraham, Journal of Computational Physics, 224(2), pp539-559 (2007).
[7] R. Du, B. Shi and X. Chen, Physics Letters A, 359(6), pp564-572 (2006).
[8] A. Fakhari and T. Lee, Phys. Rev. E 87(2), 023304 (2013).
[9] I. Halliday, X. Xu and K. Burgin, Phys. Rev. E 95, 023301 (2017).
[10] G. I. Taylor, Proc. Roy. Soc. 138 (834) pp41 (1932).
[11] E. Einstein, Ann. Physik. (19) pp. 289 (1906) and a correction to that paper Ann. Physik. (34) pp591 (1911).
[12] Y. H. Qian, D. d'Humières and P. Lallemand, Europhys. Lett. **17**, 479, (1992).
[13] H. Liu, A. J. Valocchi and Q. Kang, Phys. Rev. E 85, 046309 (2012).
[14] Y. Ba, H. Liu, J. Sun, and R. Zheng Phys. Rev. E 88, 043306 (2013).
[15] S. V. Lishchuk, C. M. Care and I. Halliday, Phys. Rev. E. 67(3), 036701(2), (2003).
[16] U. D'Ortona, D. Salin, M. Cieplak, R. B. Rybka and J. R. Banavar Phys. Rev. E. 51, 3718, (1995).
[17] M.A. Nawab S. G. Mason, Transactions of the Faraday Society, 54, pp.1712 (1958).
[18] B.K. Hur, C.B. Kim and C.G. Lee Journal of Industrial and Engineering Chemistry, 6(5), pp.318 (2000).
[19] T.G. Mason, J. Bibette and D. A. Weitz, Journal of Colloid and Interface Science, 179(2), pp.439 (1996).
[20] I. Halliday, S. V. Lishchuk, T. J. Spencer, K. Burgin and T. Schenkel, Computer Physics Communications 219, pp286 (2017).
[21] A. J. Wagner and I. Pagonabarraga, J, Stat Phys, 107(1), pp.521, (2002).
[22] L. Landau and E.M. Lifshitz, Fluid Mechanics, Ed. 2, Pergammon Press, (1966)
[23] H. Liu, A. J. Valocchi, C. Werth, Q. Kang and M. Oostrom, Advances in Water Resources, 73, pp.144 (2014).
[24] H. Liu, Y. Ju, N. Wang, G. Xi and Y. Zhang, Phys. Rev. E, 92(3), p.033306. (2015).
[25] I. Ginzburg, J. Stat. Physics, 126(1), pp.157 (2007).
[26] Y.Q. Zu, and S. He, Phys. Rev. E, 87(4), p.043301. (2013).
[27] D. Grunau, S. Chen, and K. Eggert, Physics of Fluids A: Fluid Dynamics, 5(10), pp.2557. (1993).
[28] T. J. Spencer, I. Halliday and C. M. Care, Phys. Rev. E 82, 066701 (2010).